

Compression of Fluorescence Microscopy Images Based on the Signal-to-Noise Estimation

TYTUS BERNAS,^{1,2} ELIKPLIMI K. ASEM,³ J. PAUL ROBINSON,^{2,4} AND BARTEK RAJWA^{2,4*}

¹Department of Plant Anatomy and Cytology, Faculty of Biology and Protection of Environment, Katowice, Poland

²Purdue University Cytometry Laboratories, West Lafayette, Indiana 47907-2064

³School of Veterinary Medicine, Purdue University, West Lafayette, Indiana 47907-1246

⁴Bindley Bioscience Center, Purdue University, West Lafayette, Indiana 47907-2057

KEY WORDS imaging; microscopy; photobleaching; image quality; image compression

ABSTRACT Modern microscopic techniques like high-content screening (HCS), high-throughput screening, 4D imaging, and multispectral imaging may involve collection of thousands of images per experiment. Efficient image-compression techniques are indispensable to manage these vast amounts of data. This goal is frequently achieved using lossy compression algorithms such as JPEG and JPEG2000. However, these algorithms are optimized to preserve visual quality but not necessarily the integrity of the scientific data, which are often analyzed in an automated manner. Here, we propose three observer-independent compression algorithms, designed to preserve information contained in the images. These algorithms were constructed using signal-to-noise ratio (SNR) computed from a single image as a quality measure to establish which image components may be discarded. The compression efficiency was measured as a function of image brightness and SNR. The alterations introduced by compression in biological images were estimated using brightness histograms (earth's mover distance (EMD) algorithm) and textures (Haralick parameters). Furthermore, a microscope test pattern was used to assess the effect of compression on the effective resolution of microscope images. *Microsc. Res. Tech.* 69:1–9, 2006. © 2006 Wiley-Liss, Inc.

INTRODUCTION

Digital imaging based on light microscopy has become an established technique in basic and applied biological sciences. Modern applications like high-content screening (HCS), 4D imaging, and multispectral imaging may involve collection of thousands of images in one experiment. Hence, such data are analyzed in automated ways and have to be stored using efficient image-compression techniques. Several compression algorithms have been developed for digital photography and film. Among them, lossy compression algorithms such as JPEG (ISO/IEC IS 10918-1) and JPEG2000 (ISO/IEC 15444-1) offer the highest compression ratios. However, this form of compression introduces artifacts in the images. The distortions are considered acceptable as long as the essential perceptual image quality is not decreased (Ebrahimi et al., 2004, Grgic et al., 2003). In other words, models of human vision are used to establish which image features are significant and consequently should be preserved (Ebrahimi et al., 2004). This approach is not particularly suitable for compression of microscopic data, which are analyzed in an objective (often automated) manner. It has been established that these lossy compression algorithms may introduce artifacts that impact the integrity of the scientific data contained within (Oh and Besar, 2003).

Instead, we propose three observer-independent compression algorithms designed to preserve information contained in the images. These algorithms rely on determination of signal-to-noise ratio (SNR) computed from a single image. The SNR parameter was used to

establish an appropriate compression level so as to preserve the information contained in the image. Since the SNR of microscopic images is a function of the number of collected photons, photobleaching was used to obtain images with various levels of fluorescence intensity.

MATERIALS AND METHODS

Cell Culture and Confocal Microscopy

Transformed human fibroblasts MSU 1.1 were cultured, stained with propidium iodide (PI), and imaged using a Bio-Rad MRC 1024 confocal microscope as described earlier (Bernas et al., 2004). Briefly, time series of fluorescent confocal images of equatorial sections through nuclei (thickness $\sim 1.1 \mu\text{m}$) were collected using alternately a low-intensity probing beam and a high-intensity bleaching beam. No measurable bleaching occurred when labels were excited using the probing beam alone. Images (512×512 pixels; 256 gray levels) were collected using LaserSharp 3.2 software (Bio-Rad). One image was a sum of 20 consecutive scans. PI fluorescence was detected using photomultipliers in photon-counting mode.

The array test pattern on a microscope test slide (Richardson Technologies, Inc., Fig. 2) was imaged

*Correspondence to: Bartek Rajwa, Bindley Bioscience Center, Purdue University, 1203 W. State Street, West Lafayette, IN 47907-2057.
E-mail: rajwa@flowcyt.cyto.purdue.edu

Received 10 September 2005; accepted in revised form 15 October 2005
DOI 10.1002/jemt.20259

Published online in Wiley InterScience (www.interscience.wiley.com).

using the confocal system configured, as described earlier (Bernas et al., 2004). The images of the pattern (512×512 pixels; 256 gray levels) were registered at the focal plane of maximum intensity using reflected light (488 nm). Optical-section thickness was $0.7 \mu\text{m}$ and the pixel size was $0.025 \mu\text{m}$. One image was a sum of 2 (small number of photons) or 30 (large number of photons) consecutive scans.

SNR Estimation

SNR in the Spatial Domain. The noise level was calculated using a previously described algorithm (Amer et al., 2002). First, a set of eight directional high-pass filters (3×3) was applied to an image. The resulting images were summed, and 5 pixels having the smallest sums were chosen to represent the homogenous image regions. The choice was restricted to the regions where fluorescence intensity was at least 75% of image maximum. The signal and noise were estimated using the following formulae:

$$S_s = \frac{\sum_{k=0.75I_{\max}}^{255} n_k k}{\sum_{k=0.75I_{\max}}^{255} n_k} \quad (1)$$

where S_s is the average signal; k , the pixel intensity; and n_k , the number of pixels in the k th intensity class.

$$\sigma_s = \frac{\sum_{h=1}^m \sigma_{\text{Bh}}^2}{m} \quad (2)$$

where

$$\sigma_{\text{Bh}}^2 = \frac{\sum_{i,j \in W_{ij}} (I(i,j) - \mu_{\text{Bh}})^2}{W \times W}$$

and σ_s is the noise, μ_{Bh} , the average summed intensity in the analyzed region, $I(i, j)$, the summed intensity at the (i, j) coordinates, W , the filter kernel size (3), and m , the number of selected homogenous regions (5).

SNR in the Wavelet Domain. The majority of noise present in microscope images is caused by inherent variation in the arrival rate of photons because of the quantum nature of light. Thus, Poisson noise modeling (Nowak and Baraniuk, 1999) was combined with a bivariate wavelet shrinkage algorithm (Sendur and Selesnick, 2002) to estimate SNR in microscope imaging. Average signal intensity was calculated from the resulting (denoised) images, using Eq. (1) (for $k = 30$). The absolute difference between the denoised and initial images was used as an estimate of the noise level, which was plotted against the average signal intensity.

Image Compression

Downsampling in the Spatial Domain. Performance of an optical imaging system (including a micro-

scope) is determined by its optical transfer function (OTF), (Pawley, 1995). The modulus of the OTF (modulation transfer function, MTF) characterizes amplitude (maximum to minimum intensity contrast) of a spatial frequency transferred by the system. The MTF of a confocal microscope used in further calculations is given (at the focal plane, xy) by the approximate formula below (Stokseth, 1969):

$$\text{MTF}(f_r) = 4(1 - 0.69s_{\text{ex}} + 0.0076s_{\text{ex}}^2 + 0.043s_{\text{ex}}^3) \times (1 - 0.69s_{\text{em}} + 0.0076s_{\text{em}}^2 + 0.043s_{\text{em}}^3) \quad (3)$$

where

$$s_{\text{ex}} = \frac{\lambda_{\text{ex}}}{\sin(\alpha)} f_r \quad \text{and} \quad s_{\text{em}} = \frac{\lambda_{\text{em}}}{\sin(\alpha)} f_r$$

and where f_r is the radial spatial frequency, s_{ex} , s_{em} are normalized spatial frequencies for excitation (λ_{ex}) and emission (λ_{em}) wavelengths, respectively, and α is the objective aperture half angle.

The MTF intensity (representing contrast) is plotted versus the normalized spatial frequency (s) in Figure 1. The resolution distance of the confocal microscope is determined by the maximum spatial frequency that can propagate through the system (i.e., the cutoff frequency, f_c). In the absence of noise (or when the SNR is infinite) the cutoff frequency is the point at which the MTF crosses the zero-intensity contrast line (Fig. 1). Hence, the nominal (minimal) resolution distance (d) is achieved.

$$d = 0.5 \frac{\lambda}{n \sin(\alpha)} \quad (4)$$

where

$$\lambda = 0.5 \frac{\lambda_{\text{ex}} \lambda_{\text{em}}}{\sqrt{\lambda_{\text{ex}}^2 + \lambda_{\text{em}}^2}}$$

and where d is the resolution distance and n the index of refraction

This nominal resolution is achieved if the SNR is infinite, which is not the case in actual practice. Therefore, the practical resolution was estimated by raising the zero contrast line to match the noise, as shown in Figure 1. Microscope images are registered with a number of pixels sufficient to provide adequate (Nyquist) sampling at the nominal resolution (i.e., infinite SNR). Hence, the ratio of practical to nominal resolution was used to calculate the downsampling factor for these noisy images. The downsampling (bicubic method) resulted in a lower number of pixels and thus a smaller image size. Therefore, the first of the proposed algorithms involves downsampling of the datasets collected using the sampling rates required to fulfill the Nyquist criterion at infinite SNR to the size determined by sampling rates required for practically available SNRs.

Downsampling in the Intensity Domain. Owing to the presence of noise in the images, only some inten-

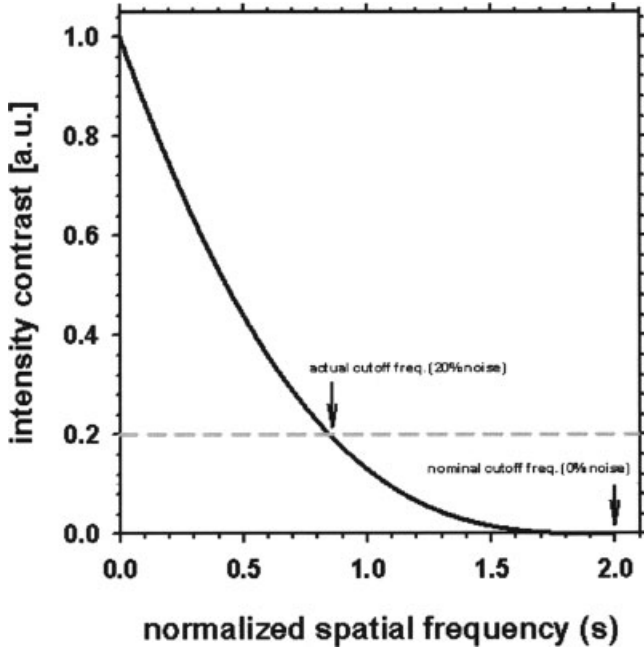


Fig. 1. Influence of noise on the cutoff frequency of the microscope MTF (continuous black line). The nominal cutoff frequency ($s = 2$ in normalized optical units) is estimated in the absence of noise at zero contrast level. Frequency-independent noise (20%, gray dashed line) is introduced by imposing a lowest limit to the contrast. The practical cutoff frequency is calculated at the point where the MTF crosses this minimum contrast level.

sity differences can be considered significant. The second proposed compression algorithm relies on the fact that the number of meaningful intensity levels is lower than the nominal dynamic range (8 bits, 256 levels). The number of levels in the images was reduced so that the difference between the nearest was twice the noise level. The following algorithm was used:

1. Calculate maximum fluorescence intensity s_{\max} in the image.
2. Calculate noise (σ) using appropriate function of fluorescence intensity $\sigma = f(s)$ so that $s = s_{\max} - \sigma$.
3. Set all the pixel values between $s - \sigma$ and $s + \sigma$ to s .
4. Set $s_{\max} = s$; if $s > 1$ go to 2.

Calculate the number of resulting intensity levels and the number of bits necessary to represent them.

The downsampled image is consequently stored using a lower than initial number of bits.

Wavelet Compression. The third proposed algorithm involves execution of the wavelet shrinkage procedure, which causes removal of those wavelet coefficients that represent noise. Hence, the number of non-zero coefficients in the wavelet transform of an image decreases. One should note that this information-preserving procedure constitutes the lossy step of the compression algorithm (the noise is the lost component). The data are then coded in lossless manner, using a wavelet representation (format), which is part of JPEG2000 specification (ISO/IEC 15444-1). Hence, only the nonzero coefficients of an image wavelet trans-

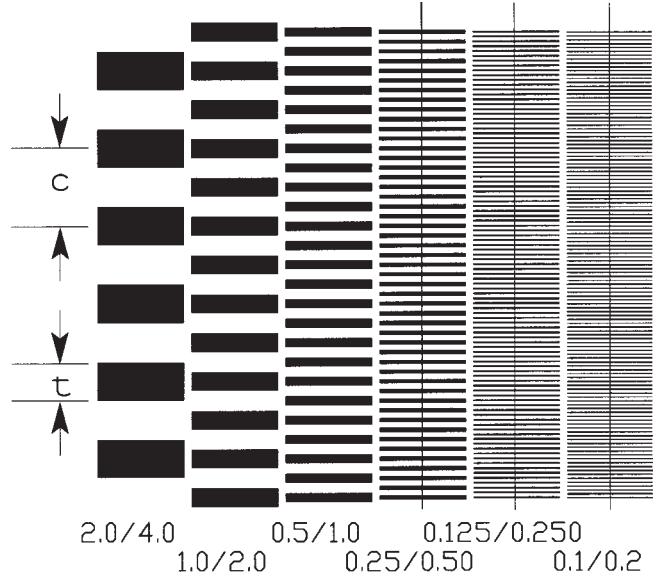


Fig. 2. Grating array test pattern. The black bars indicate the reflective (aluminum-covered) areas of the specimen, whereas regions transparent to the light are shown in white. The dimensions for each column are shown as t/c , where t is the thickness of each bar and c is the center-to-center spacing between adjacent bars (in μm).

form are stored. As a consequence, a decrease in the file size is achieved when wavelet shrinkage is applied as a preprocessing step for JPEG2000 coding.

Verification and Comparison

Intensity Distribution Comparison. Fluorescence intensity distributions (histograms) were compared for reference and compressed images using earth mover's distance (EMD) algorithm (Rumner et al., 2000). Briefly, the minimal average (per pixel) intensity change needed to transform histograms of a compressed image into the respective histogram of an uncompressed (reference) image was computed for every such image pair.

Texture Characterization. Textures of the nuclei in uncompressed and compressed images were compared using Haralick texture parameters (Tuceryan and Jain, 1998). The following parameters were used: entropy (measure of information), contrast (measure of magnitude of intensity changes), and correlation (measure of linearity of intensity changes). These parameters were calculated in the areas where the fluorescence intensity was higher than that of the background (30). Eight bits of dynamic range were used in calculations carried out for a 5-pixel distance.

Fidelity of Pattern Reproduction. Artifacts introduced by image compression were estimated using a test slide containing horizontal and vertical array patterns (Fig. 2). The patterns were comprised of bars 0.250, 0.125, or 0.100 μm thick. Intensity profiles (3-pixel width) were measured from images of the patterns registered with either large or small numbers of photons. The absolute contrast between the profile

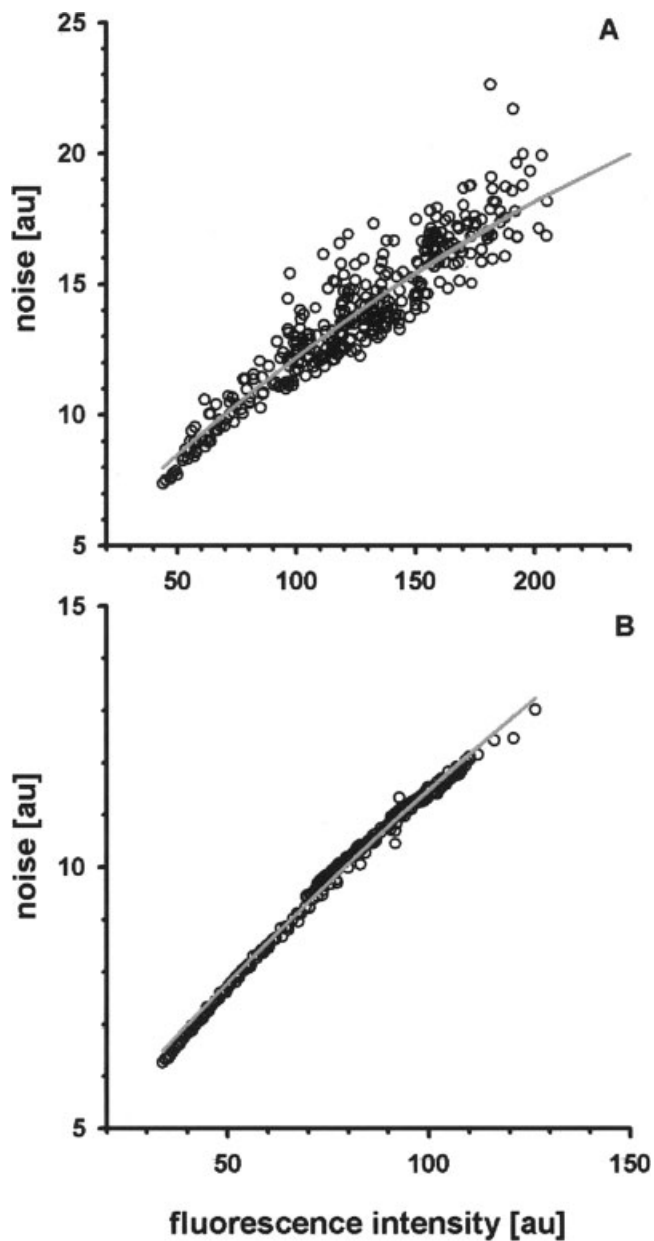


Fig. 3. Dependence of the noise on the average fluorescence intensity. The noise was estimated in spatial (A) and wavelet (B) domains. The dependence was described phenomenologically using power function of the signal (gray line).

TABLE 1. Dependence of the noise (σ) on the fluorescence intensity (I)

| Noise estimation method | Noise function |
|-------------------------|---|
| Spatial | $\sigma = -0.73 + 1.13 \times I^{0.54}$ |
| Wavelet | $\sigma = -2.91 + 2.00 \times I^{0.42}$ |

minima and maxima was calculated using the formula:

$$C_a = \frac{\sum_{p=\min}^{p=\max} |I_p - I_{p+s}|}{\max - \min} \quad (5)$$

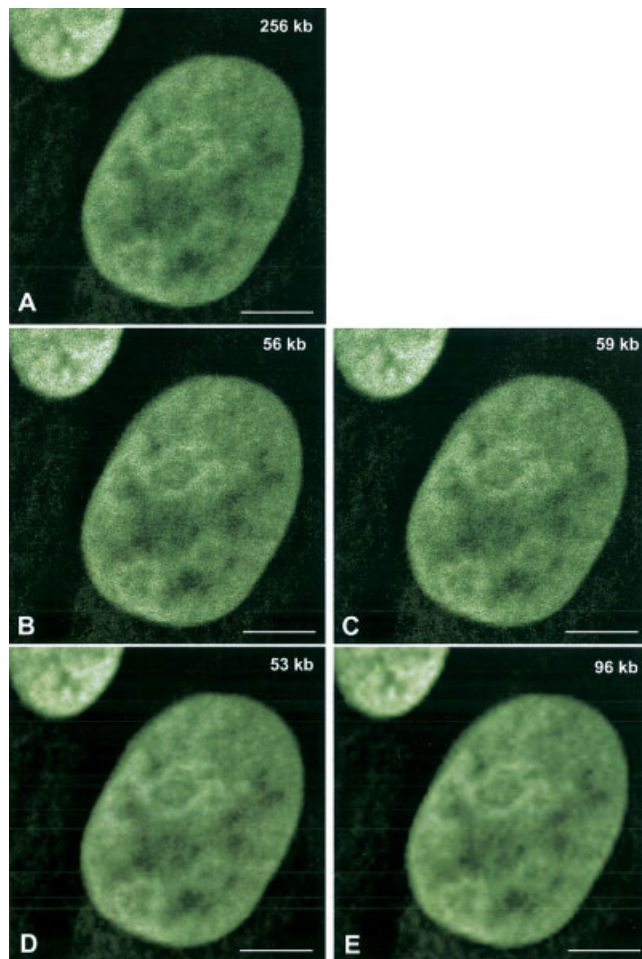


Fig. 4. Effects of compression of an image of PI-stained nuclei (A) with intensity downsampling using spatial (B) and wavelet (C) noise models, spatial downsampling (D), and wavelet shrinkage (E). File sizes in kilobytes (kb) are indicated. Bar: 5 μ m. [Color figure can be viewed in the online issue, which is available at www.interscience.wiley.com.]

where C_a is the absolute contrast; p , the index of the profile point; min , the first profile point; max , the last profile point; s , the profile shift (equal to the thickness of one or three array bars); and I , the intensity.

The normalized contrast was calculated for the compressed images using the formula:

$$C_r = \frac{C_a^{cm}}{C_a^{noc}} \quad (6)$$

where C_r is the relative contrast; C_a^{cm} , the absolute contrast for a compressed image; and C_a^{noc} , the absolute contrast for its noncompressed counterpart.

Hence, the relative contrast was equal to unity if no artifacts were introduced by a compression algorithm.

RESULTS

Dependence of Noise on Fluorescence Intensity

Changes in fluorescence intensity were followed by changes in the noise level, calculated using both spatial-domain (Fig 3A) and wavelet-based (Fig. 3B) algo-

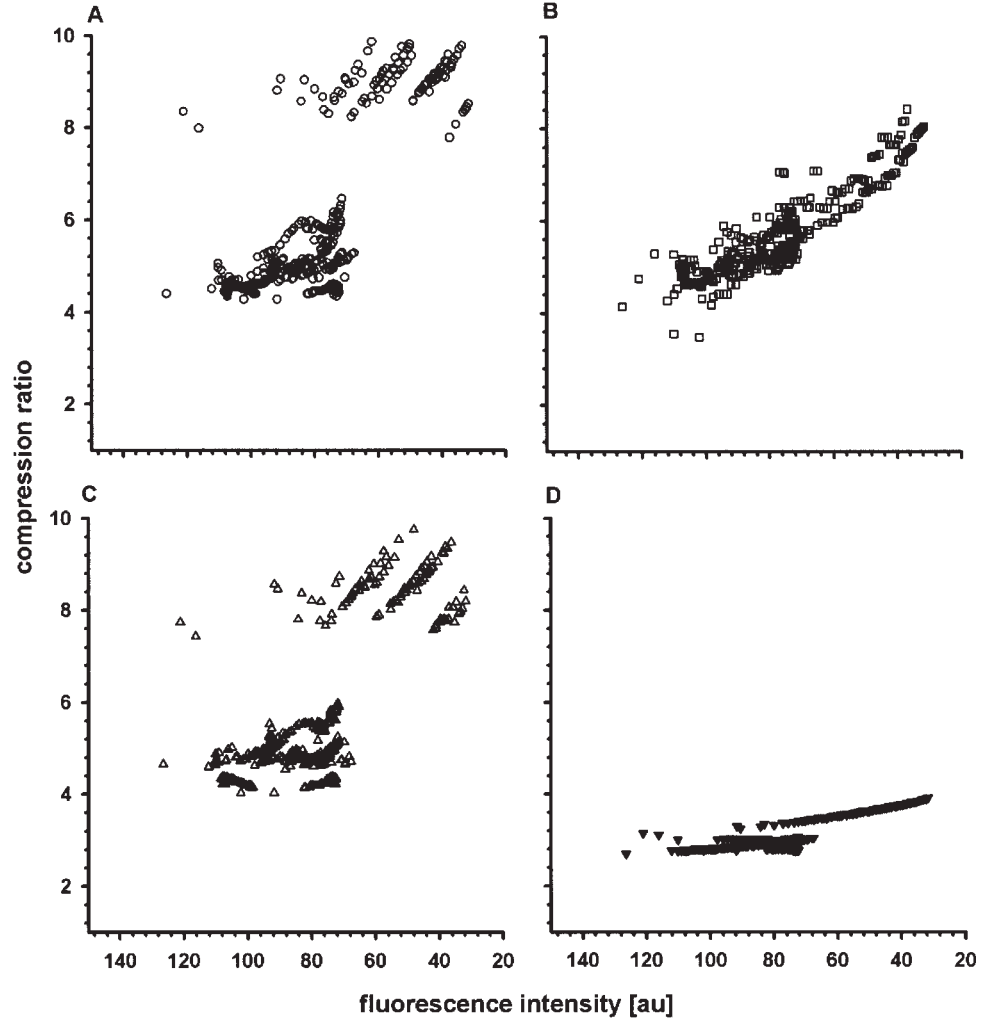


Fig. 5. Influence of fluorescence intensity on the compression efficiency of images of PI-stained nuclei. The images were compressed by intensity downsampling using spatial (A) and wavelet (B) noise models, by spatial downsampling (C), and by wavelet shrinkage (D).

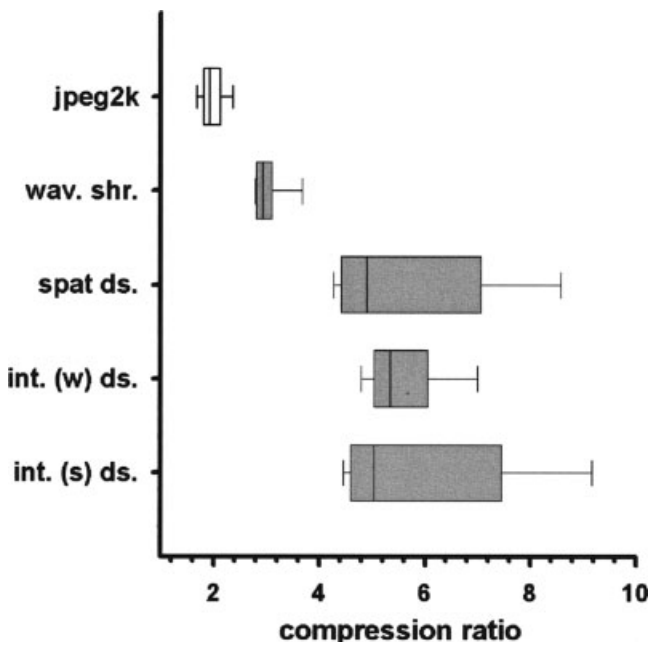


TABLE 2. Alterations of fluorescence intensity distributions (histograms) in compression, as measured using EMD. Data are expressed as the average \pm standard deviation

| Compression method | EMD |
|--|-----------------|
| Intensity downsampling (spatial noise) | 5.52 ± 0.66 |
| Intensity downsampling (wavelet noise) | 5.17 ± 0.67 |
| Spatial downsampling | 1.66 ± 0.28 |
| Wavelet shrinkage | 1.51 ± 0.24 |

gorithms. The noise could be modeled using a square-root function of fluorescence intensity in both cases (Figs. 3A and 3B, Table 1). Furthermore, both methods gave comparable noise levels for a given fluorescence intensity, indicating that noise constitutes a significant part of image data. Hence, one may postulate that only part of image data constitutes information. Three

Fig. 6. Overall compression efficiency of intensity downsampling using spatial and wavelet noise models, spatial downsampling, and wavelet shrinkage. Data range indicated with bars, 10th and 90th percentiles with gray boxes, and median compression ratios with vertical lines.

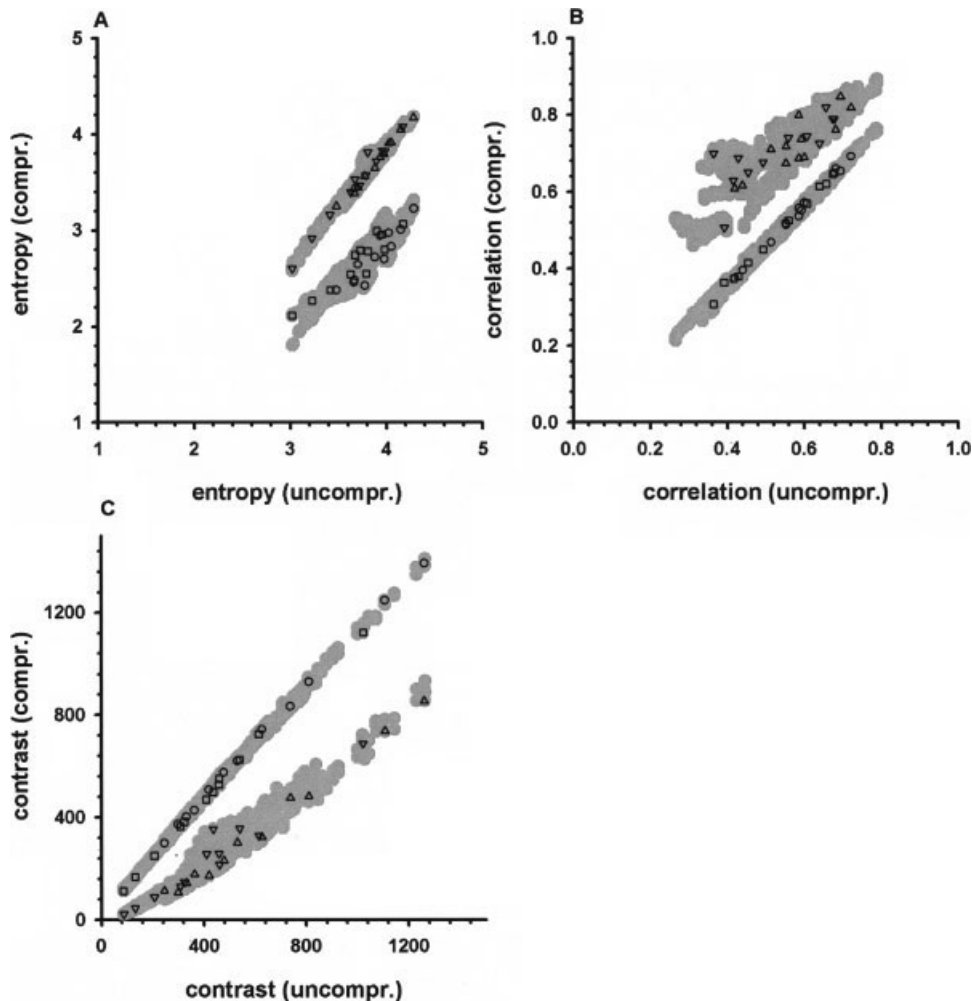


Fig. 7. Influence of compression on textures in the images of PI-stained nuclei, determined using Haralick parameters entropy (A), correlation (B) and contrast (C). The images were compressed by intensity downsampling using spatial (circles) and wavelets (squares) noise models, by spatial downsampling (triangles up), and by wavelet shrinkage (triangles down). 10% randomly chosen images representing sets are indicated using black symbols, whereas the whole sets are depicted as grey areas.

image-compression techniques described in the Materials and Methods section attempt to exploit this redundancy.

Performance of Wavelet-Shrinkage, Spatial, and Intensity Downsampling

Biological Images. A set of fluorescence images of PI-stained nuclei was compressed using the three proposed algorithms (see Materials and Methods), as illustrated in Figure 4. It should be noted that no gross artifacts were generated and efficient compression was achieved. These two aspects were studied in detail using a set of 470 images containing various numbers of nuclei and characterized by different intensity levels.

The compression ratio of all three algorithms increased with decreasing fluorescence intensity for all the algorithms (Fig. 5). It should also be noted that this dependence was more pronounced for algorithms where wavelet-based noise estimation was used (Figs. 5B and 5D), than for those involving spatial-based (Figs. 5A and 5C) noise estimation. The median compression efficiency increased in the following order:

wavelet shrinkage < intensity downsampling < spatial downsampling (Fig. 6). Algorithms based on noise estimation in the spatial domain exhibited more variability in compression rates compared with wavelet-based routines. Nonetheless, all the proposed algorithms produced images significantly smaller than that of raw datasets encoded using lossless JPEG2000. Obviously, the images can be compressed further by applying JPEG2000 lossless encoding to the denoised or downsampled files.

The compressed images were compared quantitatively with their uncompressed counterparts with respect to the intensity distribution and texture. Average EMD (see Materials and Methods) is small for wavelet compression and spatial downsampling, indicating that no significant changes were introduced (Table 2). More pronounced changes were detectable in the histograms of images subjected to intensity downsampling, which is a direct consequence of the reduction in the number of intensity levels.

Comparison of the Haralick texture parameters entropy, correlation, and contrast at the 5-pixel distance (Fig. 7) between compressed and uncompressed images indicates that microscopically resolved details

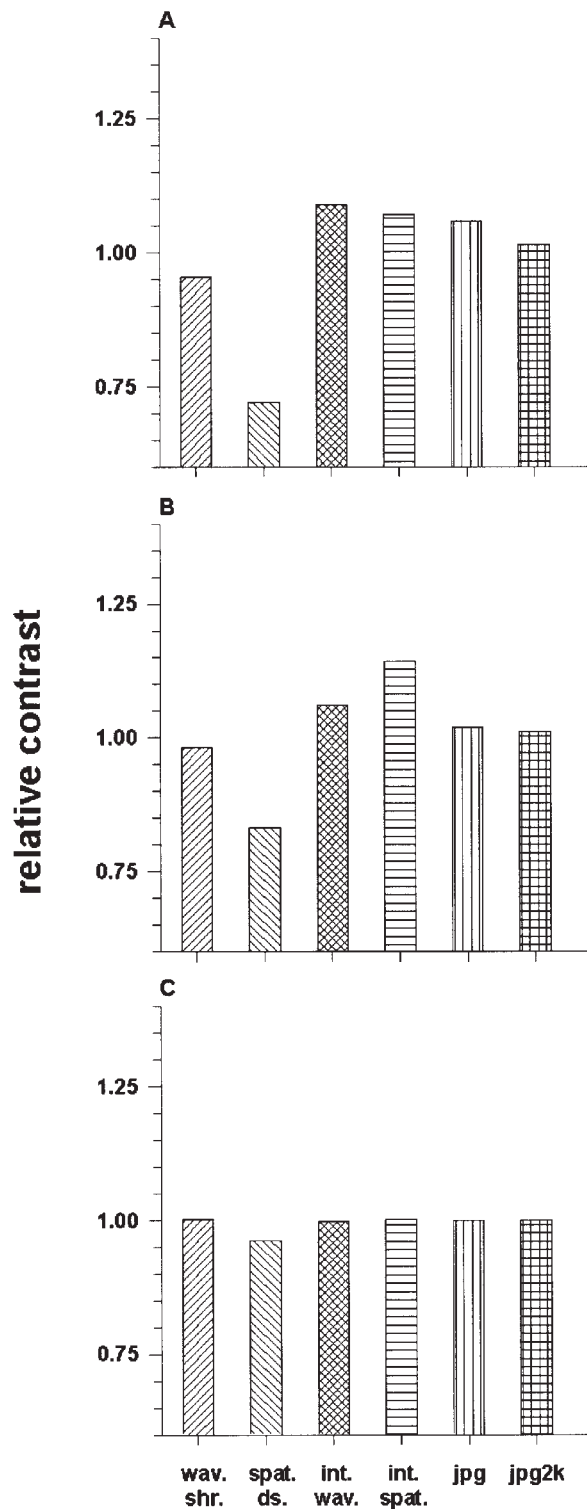


Fig. 8. Influence of compression on images of the array test pattern registered with a large number of photons (average of 72.8/pixel). The fidelity of reproduction of the test pattern was estimated using relative contrast between bright and the dark bars (see Materials and Methods). The contrast was calculated shifting the pattern with respect to itself by one bar width. The respective widths were 0.100 μm (A), 0.125 μm (B), and 0.250 μm (C). The following adaptive compression methods were analyzed: wavelet denoising (slash pattern), spatial downsampling (backslash pattern), intensity downsampling using wavelet (oblique grid), and spatial (horizontal stripes) noise models. Effects of compression using JPEG (vertical stripes) and JPEG2000 (vertical grid) are shown for comparison.

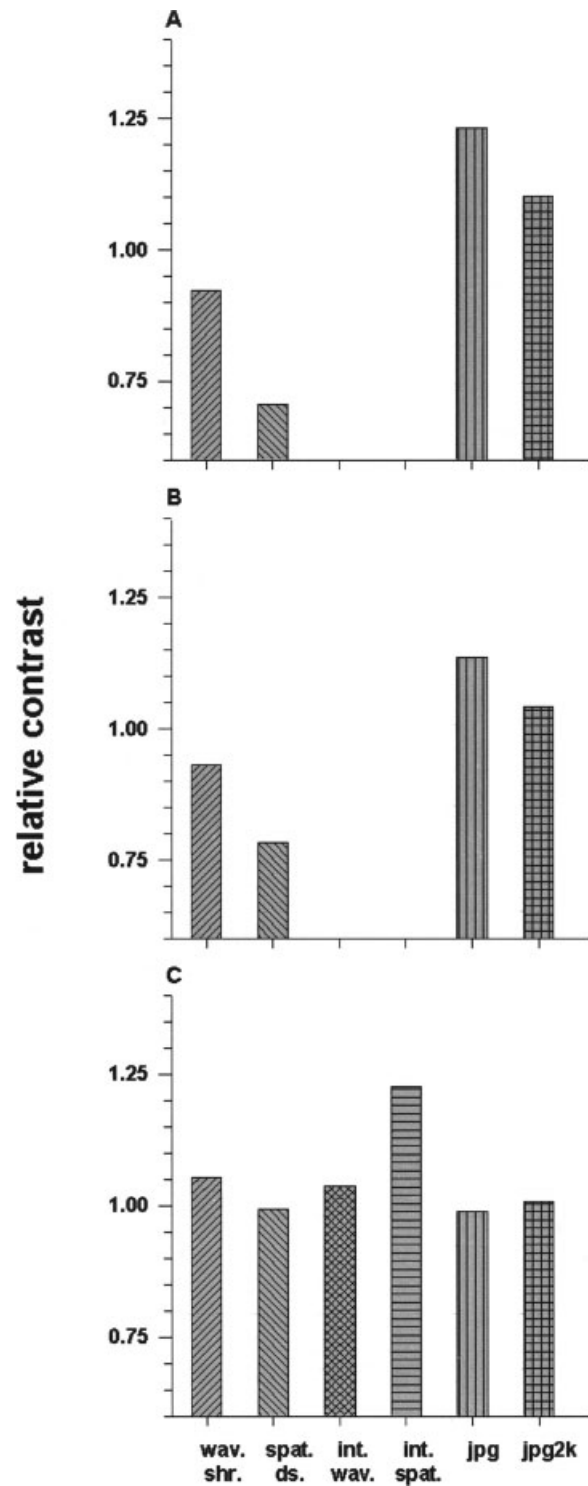


Fig. 9. Influence of compression on images of the array test pattern registered with a small number of photons (average of 4.1/pixel). The fidelity of reproduction of the test pattern was estimated using relative contrast between bright and dark bars (see Materials and Methods). The contrast was calculated shifting the pattern with respect to itself by one-bar width. The respective widths were 0.100 μm (A), 0.125 μm (B), and 0.250 μm (C). The following adaptive compression methods were analyzed: wavelet denoising (slash pattern), spatial downsampling (backslash pattern), intensity downsampling using wavelet (oblique grid), and spatial (horizontal stripes) noise models. Effects of compression using JPEG (vertical stripes) and JPEG2000 (vertical grid) are shown for comparison.

were only slightly affected. Intensity downsampling did lower the entropy (which is a measure of information). On the other hand, spatial downsampling and wavelet shrinkage resulted in an increase of correlation, while contrast was decreased.

Microscope Test Patterns. Compressed images of an array grid pattern (Fig. 2) were compared with their noncompressed counterparts to estimate the influence of the algorithms described here on the reproduction fidelity of details of known size. These effects, quantified using contrast between the reflective and transparent regions of the patterns (see Materials and Methods), are shown in Figures 8 and 9. Wavelet shrinkage did not introduce significant changes in the images of the finest ($0.100\ \mu\text{m}$) grating, as demonstrated by the relative contrast close to unity (Figs. 8 and 9). Spatial downsampling resulted in a marked decrease of this parameter, which is an indicator of pattern blurring. Intensity downsampling, JPEG, and JPEG2000 did not introduce large distortion in the pattern imaged with large number of photons (Fig. 8). However, these algorithms did not preserve small details registered using a small number of photons (Fig. 9). Changes in contrast were manifested at both short (1 bar length, Figs. 8 and 9) and long pattern shifts (3 bar lengths, data not shown). This indicates that the artifacts were introduced into the whole pattern at regular intervals (i.e., they were periodic). JPEG spatial downsampling, intensity downsampling, and both JPEG variants exhibited better reproduction fidelity in case of a coarser ($0.125\ \mu\text{m}$) array grating (Figs. 8B and 9B). Nonetheless, intensity downsampling failed in accurate reproduction of dim details. The best fidelity was provided by wavelet shrinkage, as in the case of the finest grating. The coarsest pattern was reproduced accurately by all the algorithms analyzed (Figs. 8C and 9C). Inaccuracy was manifested only when the pattern was registered with a small number of photons and compressed using intensity downsampling with spatial noise estimation.

DISCUSSION

The nature of the dependence of image noise on fluorescence intensity indicates that the main noise component was of photonic origin. This notion is supported by the fact that similar noise levels were estimated using spatial (total noise) and wavelet (photonic noise) methods. The noise constituted a significant part of the total fluorescence intensity. Hence, one may postulate that the image data contained significant redundancy with regard to the information content. This redundancy was exploited by the three proposed methods to obtain better compression efficiency than is offered by standard lossless compression algorithms. As expected, the compression efficiency increased with decreasing image brightness (i.e., decreasing SNR). Thus, the proposed algorithms are actually adaptive to the amount of information present in the images.

Compression using wavelet shrinkage and spatial downsampling did not introduce significant changes to fluorescence intensity distributions (histograms), as indicated by a small EMD. Such changes were more pronounced in the case of intensity downsampling. It

should be noted that these algorithms perform operations equivalent to histogram binning. Nonetheless, the EMD in this case is small when compared with the average intensity bin size. This fact indicates that the binning was fine enough to represent the histogram in a faithful manner.

Wavelet shrinkage and spatial downsampling did not influence image texture entropy, whereas intensity downsampling resulted in a small decrease for this parameter, possibly because of nonuniform intensity binning. Intensity downsampling did not affect the correlation and contrast. The other two algorithms resulted in a slight increase in the correlation, while the contrast was slightly decreased. It should also be noted that these two techniques made use of correlation of fluorescence intensity between pixels. Nonetheless, in general, we believe that none of the proposed algorithms significantly altered even the smallest details that could be resolved with the fluorescence microscopy employed here. Thus, the scientific integrity, as opposed to the “image presentation,” was maintained.

Compression using wavelet shrinkage did not introduce any artifacts to the images of periodic grating arrays. The response of an imaging system to such patterns is an estimate of the MTF. The finest of the patterns (bar thickness, $0.100\ \mu\text{m}$) was characterized by a spatial frequency of $5.0\ \mu\text{m}^{-1}$, which was close to the microscope cutoff frequency ($5.7\ \mu\text{m}^{-1}$). Therefore, one may claim that wavelet shrinkage does not impair resolution of microscope imaging. Intensity downsampling and both JPEG variants distorted dim details and to a lesser extent bright details at this high spatial frequency. On the other hand, spatial downsampling resulted in blurring of the finest details. One should note, however, that the transfer efficiency decreases as spatial frequencies approach the cutoff (Fig. 1). Thus, the frequencies close to the cutoff constitute only a small fraction of the energy that is contained in the microscopic images. Consequently, it is conceivable that distortions of nuclei images caused by MTF alteration at these high frequencies might be nondetectable. Grating arrays characterized by lower spatial frequencies were reproduced accurately in the images compressed using all the algorithms except intensity downsampling. Use of these methods resulted in inaccuracies when the intensity level was low. It is not surprising because relative error (which results from the downsampling) increases as the intensity decreases.

The actual compression efficiency is lower than that theoretically predicted for spatial and intensity downsampling. One may envisage that an alternative image file structure (i.e., allowing arbitrary choice of dynamic range, e.g., 5-bit) could improve the practical performance of downsampling-based methods. No such predictions could be made for wavelet shrinkage. However, we believe that the construction of a JPEG2000-compliant routine, which would utilize the denoised wavelet image representation, could result in an increase of the compression ratio, while maintaining the essential integrity of the inherent scientific data. Such a solution may well be attractive to those requiring 21 CFR part 11 compliance for their data storage and compression.

ACKNOWLEDGMENTS

This work was partially supported by the Foundation for Polish Science (TB).

REFERENCES

- Amer A, Dubois E, Mitiche A. 2002. Reliable and fast structure-oriented video noise estimation. *Proc IEEE Int Conf Image Process*, Rochester, NY. 1:840–843.
- Bernas T, Zarebski M, Cook PR, Dobrucki JW. 2004. Minimizing photobleaching during confocal microscopy of fluorescent probes bound to chromatin: role of anoxia and photon flux. *J Microsc* 215:281–296.
- Ebrahimi F, Chamik M, Winkler S. 2004. JPEG vs. JPEG2000: An objective comparison of image encoding quality. *Proc SPIE Appl Digit Image Process* 5558:300–3008.
- Grgic S, Mrak M, Grgic M, Zovko-Cihlar B. 2003. Comparative study of JPEG and JPEG2000 image coders. *Proc 17th Conf Appl Electromag Commun*, Dubrovnik, Croatia. pp 109–112.
- ISO/IEC IS 10918–1. ITU-T Recommendation T. 81 Part 1: The basic JPEG standard, which defines many options and alternatives for the coding of still images of photographic quality.
- ISO/IEC 15444–1. ITU-T Recommendation T. 800. International Organization for Standardization. JPEG 2000 Image coding system: core coding system.
- Nowak R, Baraniuk RG. 1999. Wavelet domain filter for photon imaging systems. *IEEE Trans Im Proc* 8:1–24.
- Oh TH, Besar R. 2003. JPEG2000 and JPEG: image quality measures of compressed medical images. *NCTT Proc 4th National Conf Telecommun Tech*, Shah Alam, Malaysia. pp 31–35.
- Pawley JB. 1995. *Handbook of biological confocal microscopy*. New York: Plenum.
- Runner Y, Tomassi C, Leonidas JG. 2000. Earth mover's distance as a metric for image retrieval. *Int J Comput Vis* 40:99–121.
- Sendur L, Selesnick IW. 2002. Bivariate image shrinkage with local variance estimation. *IEEE Trans Signal Process* 50:2744–2756.
- Stokseth P. 1969. Properties of defocused optical systems. *J Opt Soc Am* 59:1314–1421.
- Tuceryan M, Jain AK. 1998. Texture analysis. In: Chen CH, Pau LF, Wang PSP, editors. *The handbook of pattern recognition and computer vision*. River Edge, New Jersey: World Scientific. pp. 207–248.